HHS Public Access

Author manuscript

Biomater Sci. Author manuscript; available in PMC 2019 November 20.

Published in final edited form as:

Biomater Sci. 2018 November 20; 6(12): 3121–3125. doi:10.1039/c8bm00851e.

Microfluidics-enabled rapid manufacturing of hierarchical silica-magnetic microflower toward enhanced circulating tumor cells screening

Nanjing Hao[1], **Yuan Nie**[1], **Amogha Tadimety**[1], **Ting Shen**[2], and **John X.J. Zhang**[1]

[1]Thayer School of Engineering, Dartmouth College, 14 Engineering Drive, Hanover, New Hampshire 03755, United States. john.zhang@dartmouth.edu

[2]NanoLite Systems, 1521 Concord Pike, Wilmington, DE 19803, United States.

Abstract

The emergence of microfluidic techniques provides new opportunities for chemicals synthesis and biomedical applications. Herein, we first develop a microfluidics-based flow and sustainable strategy to synthesize hierarchical silica-magnetic microflower with unique multilayered structure for the efficient capture of circulating tumor cells through our engineered microfluidic screening chip. The production of microflower materials can be realized within 94 milliseconds and a yield of nearly 5 grams per hour can be achieved. The enhanced bioaccessibility of such multilayered microflower toward cancer cells (MCF-7 and MDA-MB-231) is demonstrated, and the cancer cell capture efficiency of this hierarchical immunomagnetic system in clinical blood samples is significantly increased compared with standard CellSearch™ assay. These findings bring new insights for engineering functional micro-/nanomaterials in liquid biopsy.

Graphical Abstract

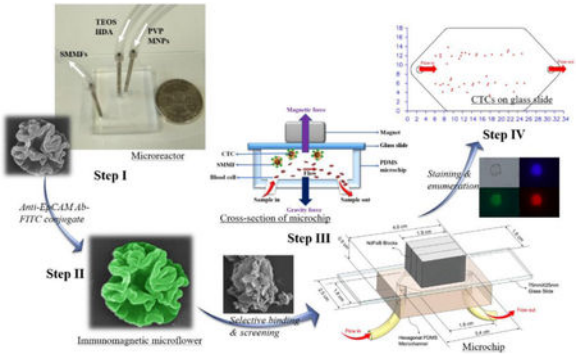

Microfluidics-enabled rapid manufacturing of hierarchical silica-magnetic microflower was developed for improving the screening efficiency of circulating tumor cells

Conflicts of interest

There are no conflicts of interests to declare.

Electronic Supplementary Information (ESI) available: [details of any supplementary information available should be included here].

During the last decade, circulating tumor cells (CTCs) have received considerable attention as non-invasive liquid biopsy biomarkers for early detection, diagnosis, and monitoring of cancer. Different from conventional tissue biopsies that are mostly risky, costly, and time-consuming, CTCs that shed off from the tumor site into the bloodstream facilitate convenient, inexpensive, and real-time monitoring of tumor evolution and therapeutic efficacy, providing the great potential to improve cancer diagnosis and treatment.[1–3] Although CTCs occur at relatively low levels in the background of millions of blood cells,[4] continuous effort has been made on the development of new methods and techniques that enable the enrichment and analysis of CTCs, such as microfiltration,[5] dielectrophoresis,[6] hydrodynamic sorting,[7] acoustophoresis,[8] nucleic acid-based assays,[9] and antibody-based immunoassays.[10–12] Among these, magnetic nanoparticles (MNPs)-based immunomagnetic assay has received great interest from researchers due to their unique magnetic response for separation and antibody-enabled selective binding of CTCs, which promise relatively higher specificity, better sensitivity, and higher throughput.[13,14] The most well-known CellSearch™ system that uses EpCAM-conjugated ferrofluid (Veridex Ferrofluid™) to capture CTCs and subsequently visualizes them via staining was the first immunomagnetic assay approved by the US Food and Drug Administration.[2,3] This standard protocol provides important prospects for creating new immunomagnetic platforms with improved outcomes in liquid biopsy.

In recent years, more and more evidence from both theoretical and experimental aspects has revealed that particle designs play significant roles in their biological performance.[15–19] Particle shape as an important parameter has also gained substantial attention. It has been found that non-spherical particles, especially those having hierarchical structures, generally possess more advanced biological behaviors than their spherical counterparts, such as higher cellular binding efficiency, larger transmembrane capacity, and longer circulation time.[20–22] Therefore, the screening performance of CTCs may be well regulated and even greatly improved through the rational design and controllable synthesis of novel hierarchical immunomagnetic materials. However, due to limited methods and the intrinsic problems from conventional batch reactors, there is still a big challenge to fabricate hierarchical materials in an efficient, reproducible, and scalable manner.[23,24] Alternatively, the emergence of microfluidic techniques provides new opportunities for chemical synthesis and biomedical applications.[25] In particular, microfluidics-based microreactors have many appealing features that batch reactors can hardly achieve, for example, greatly reduced reactor dimensions and automated operations for minimized local variations, intensive mixing of chemical reactants for high yields, rapid reaction kinetics for fast screening and optimization of synthesis parameters, and elevated pressure and temperature in confined space for reactions with harsh conditions (explosive, toxic, or flammable).[26–28]

In this study, based on the merits of microfluidics, we first developed an efficient, reproducible, and scalable strategy to synthesize hierarchical silica-magnetic microflower (SMMF) with multilayered structures from miniaturized microreactor (Figure 1, Step I). We then conjugated the EpCAM antibody on SMMF surface (Figure 1, Step II) and examined its CTCs screening performance using our developed CellRich™ microchip (Figure 1, Step III). The captured cells were finally identified and enumerated (Figure 1, Step IV) and the results were compared to the standard CellSearch™ system.

Microfluidics-enabled flow and continuous synthesis of hierarchical microflower materials with unique multilayered structures was realized by a five-run spiral-shaped microreactor with two inlets and one outlet (Figures S1 and 2A). The spiral-shaped microchannel was chosen mainly because of its relatively rapid and intensive mixing performance for the chemical reagents.[29–31] The smallest diameter of microchannel is 5.25 mm and then it gradually increases from 11.0 mm to 22.2 mm with an increment of 1.4 mm for each half run. The height and the width of the microchannel are 50 and 500 μm, respectively. The two inlet flows, one containing tetraethyl orthosilicate (TEOS, 0.34 M in ethanol) and hexadecylamine (HDA, 0.02 M in ethanol) and the other having polyvinylpyrrolidone (PVP, 0.02 M in water) and magnetic nanoparticles (MNPs, 2 mg/mL in water), were pumped (Pump 33 DDS, Harvard Apparatus) into the microreactor at room temperature and the microflower product was collected at the outlet (Figure 2A).

Owing to their unique properties, microreactors provide great promises to synthesize chemicals in an efficient, reproducible, and scalable manner. To demonstrate this, we first examined the capacity of such spiral-shaped microreactor for producing silica microflower when the flow rates of TEOS/HDA and PVP inlet solutions were both 4 mL/min. A complete mixing of reaction fluids within about one circle of the spiral was revealed by COMSOL analysis (Figure 2B, see simulation details in SI), and the product can be obtained within 94 milliseconds (see calculation details in SI), showing the ultrafast reaction kinetics inside the microchannels. As shown in Figures 2C-F, well-defined silica microflower with unique multilayered structures having an average size of ~2 μm was obtained in a large scale, the production can achieve nearly 5 grams per hour with over 95% yield. Such three-dimensional hierarchical microflower structures were further clearly revealed by the transmission scanning microscopy (TEM, Figure 2G), and there are no obvious batch-to-batch differences because of the automatic operations in confined microchannels. These results demonstrated that, compared with conventional batch reactors, microfluidic reactors provide significant advantages for accelerating and scaling-up the production of micro-/nanostructures. In addition, we investigated the roles of HDA and PVP in the formation of silica microflower. There were no obvious materials formed in the absence of HDA, while some irregular and aggregated materials with typical folds were obtained without the addition of PVP (Figure S2), revealing the roles of HDA and PVP as structural-directing agent and structural-stabilizing agent, respectively. However, if further increasing the flow rate to 6 mL/min, a mixture of microflower and spherical structures was yielded (Figure S3). To fabricate the silica-magnetic microflower (SMMF), FeCo MNPs with an average size of ~15 nm and saturation magnetism value of ~74 emu/g were synthesized (Figures S4 and S5)[32,33] and then added into the inlet flow of PVP while keeping the other inlet flow the same (4 mL/min). It was found that hierarchical microflower structures can still be obtained with MNPs relatively evenly distributed inside the silica matrix (Figure 2H), which was further confirmed by energy dispersive X-ray spectroscopy (EDS) element mapping analysis (Figures 2Ia-e). The saturation magnetism value of the resulting magnetic microflower was measured to be ~13 emu/g (Figure S6) and SMMF can be easily separated using an external magnet (Figure S7).

Due to its unique hierarchical multilayers, SMMF is expected to significantly increase the bioaccessibility toward cancer cells and thus enhance the circulating tumor cells screening

efficiency. To demonstrate this, we first functionalized the SMMF particle surface with FITC-conjugated Anti-EpCAM (SMMF-EpCAM, see details in SI),[34,35] which is commonly used in current immunomagnetic assays including the standard CellSearch™. The FITC conjugates of antibody help not only on confirming the successful functionalization (Figure S8), but also on tracking the particle locations fluorescently after in contact with cancer cells. As comparison, two different kinds of human breast cancer cell lines (MCF-7 and MDA-MB-231) were used, where MCF-7 cell and MDA-MB-231 cell are $EpCAM^{pos}$ and $EpCAM^{low/neg}$, respectively.[36] Cytotoxicity assay with a CCK-8 kit revealed that SMMF-EpCAM has good biocompatibility even when the particle concentration was up to 250 μg/mL (Figure S9). We then investigated the effect of treatment time and concentration of SMMF-EpCAM on the cellular binding performance using flow cytometry (Figures 3A-B), fluorescent microscopy (Figure 3C), and SEM (Figure 3D). Flow cytometry and fluorescent microscopy can quantitatively and qualitatively measure the fluorescent intensity of cells, respectively, while SEM could provide direct information of the interactions between particles and cells. As shown in Figure 3A, flow cytometry results demonstrated that both MCF-7 and MDA-MB-231 cells exhibit fast binding kinetics within the first 30 min and nearly continuous incremental binding behaviour in the following several hours. It is noted that, as expected, MCF-7 cells have an obvious higher binding activity of SMMF-EpCAM than MDA-MB-231 cells, which was further confirmed by the fluorescent microscopy results (Figure 3C). In addition, flow cytometry results revealed that the cellular binding amount of SMMF-EpCAM by MCF-7 and MDA-MB-231 cells was not only cell type-dependent but also increased with increasing particle concentrations (Figure 3B). We also used SEM to directly investigate the detailed interactions of particles with cells. As shown in Figure 3D, at a particle concentration of 25 μg/mL, there were very few microflowers on the cell surfaces. When increasing the particle concentration to 100 μg/mL and above, a large numbers of microflowers were obviously observed on the cell surfaces, especially for MCF-7 cells. These results demonstrated that such unique microflower structure interacts with cancer cells in a fast and efficient manner, which may improve the screening performance when applying them into liquid biopsy.

Owing to the enhanced bioaccessibility from hierarchical multilayered structure, such microflower may show great performance in the screening of CTCs. To demonstrate this, we examined the capture and enrichment efficiency of SMMF-EpCAM in tumor cells-spiked whole blood samples through our developed microfluidic screening system (CellRich™, Figure S10).[37–40] As demonstrated, the combination of microfluidics and immunoassays affords a promising platform for sensitive, high throughput, low sample consumption, and automatic point-of-care diagnosis.[12,41] The design parameters and working principle of our microchip are shown in Figures 4A-B. A special polydimethylsiloxane (PDMS) cartridge is bound to a standard glass slide forming a hexagonal microchamber. Three permanent magnets are placed outside the PDMS cartridge with alternate polarities, and the blood samples are introduced into the microchannel by an external syringe pump. When blood samples flow through the microchannel, immunomagnetic particles-bound cancer cells can be magnetically captured and deposited onto the glass slide surface, while the normal hematocytes flow out of the microchannel. After the screening process, the captured cells fixed on the glass slide surface can be immunofluorescently stained for identification,

enumeration, and further analysis. Here, we chose to spike relatively rare number of MCF-7 and MDA-MB-231 cells (~50 cells) into healthy (non-cancerous) human whole blood to examine the screening capacity of SMMF-EpCAM during the early stage of cancer (see details in SI). Capture rate is defined as the ratio of captured cancer cell numbers from the screening blood samples to the average cell numbers counted on three control glass slides that are prepared from the same cell suspension as the blood samples spiked. The captured cancer cells on the glass slide can be easily identified by the morphology or the typical green fluorescent signal from SMMF-EpCAM under a microscope. To avoid the possible interference of dust and white blood cells, we further used Hoechst 33342 (blue-fluorescent DNA probe) and Anti-Pan Cytokeratin eFluor® 615 (red-fluorescent cytokeratin probe) to immunofluorescently stain the experimental slides. With these treatment, cancer cells exhibit recognizable blue, red, and green color (Figure 4C), we thus can accurately distinguish the cancer cells and calculate the capture rates. The results in figure 4D show that SMMF-EpCAM has greatly enhanced the capture rates (>85%) of MCF-7 cells at the screening flow rates of 2.5 mL/h and 5 mL/h, whereas, the capture rates of SMMF-BSA and Veridex Ferrofluid (EpCAM-conjugated from CellSearch™, Figure S11) were relatively low (~40–50%). In addition, SMMF-EpCAM and SMMF-BSA have similar capture rates of MDA-MB-231 cells (~30–40%) at the screening flow rates of 2.5 mL/h and 5 mL/h, and still greatly higher than that of Veridex Ferrofluid (<15 %). We further used SEM to observe the interactions between the captured cancer cells and the immunomagnetic particles. Due to its unique multilayered structure, SMMF-EpCAM can be easily identified under SEM, providing a convenient way to track the cancer cells. As shown in figures 4E-F, MCF-7 cells could bind more numbers of SMMF-EpCAM than MDA-MB-231 cells. Compared with SMMF-BSA and Veridex Ferrofluid, SMMF-EpCAM exhibited obviously larger binding amount of the captured cancer cells, especially MCF-7 cells (Figure S12). These results are in good agreement with the observations of microflower-cell interaction from figure 3 and clearly demonstrated their capture rate difference from figure 4D, showing the promising performance of such hierarchical multilayered microflower structure in CTCs screening.

Conclusions

In summary, we first developed a microfluidics-based flow and continuous strategy for accelerating and scaling-up the production of hierarchical microflower with unique multilayered structure and employed it as a promising immunomagnetic probe for circulating tumor cells screening through our developed microfluidic chip. Using the miniaturized spiral-shaped microreactor, the microflower material could be produced within 94 ms at a reagent flow rate of 4 mL/min and the production yield achieved nearly 5 grams per hour. Relying on its enhanced bioaccessibility from the multilayered structure, SMMF-EpCAM showed relatively fast cellular binding kinetics during the first 30 min, and the cellular binding amount was particle concentration-dependent. Through our screening microchip, it was found that SMMF-EpCAM exhibited greatly higher capture rates than SMMF-BSA and Veridex Ferrofluid towards tumor cells (especially MCF-7 cells)-spiked whole blood samples at different screening flow rates. These findings bring new insights not only for the sustainable and controllable synthesis of functional micro-/nanomaterials, but

also for the rational design of particulate systems in diverse fields, such as separation and purification, catalysis, liquid biopsy, and biosensor.

Supplementary Material

Refer to Web version on PubMed Central for supplementary material.

Acknowledgements

This work is sponsored by the NIH Director's Transformative Research Award (R01HL137157), and NSF grants (ECCS 1128677, 1309686, 1509369). We gratefully acknowledge the support from the Electron Microscope Facility at Dartmouth College. We thank Professor Ian Baker and Bradley Reese for their help in the magnetic hysteresis measurement, Professor Margie Ackerman for the flow cytometry analysis, and Abigail Brunelle and Mary McGuigan for preparing the whole blood samples.

References

1. Alix-Panabières C and Pantel K, Nat. Rev. Cancer, 2014, 14, 623–631. [PubMed: 25154812]
2. Hao N and Zhang XJ, Sep. Purif. Rev, 2018, 47, 19–48.
3. Tadimety A, Closson A, Li C, Yi S, Shen T and Zhang XJ, Crit. Rev. Clin. Lab. Sci, 2018, 55, 140–162. [PubMed: 29388456]
4. Lu Y, Liang H, Yu T, Xie J, Chen S, Dong H, Sinko PJ, Lian S, Xu J, Wang J, Yu S, Shao J, Yuan B, Wang L and Jia L, Cancer, 2015, 121, 3036–3045. [PubMed: 25945459]
5. Park JM, Lee JY, Lee JG, Jeong H, Oh JM, Kim YJ, Park D, Kim MS, Lee HJ, Oh JH, Lee SS, Lee WY and Huh N, Anal. Chem, 2012, 84, 7400–7407. [PubMed: 22881997]
6. Gascoyne PRC, Noshari J, Anderson TJ and Becker FF, Electrophoresis, 2009, 30, 1388–1398. [PubMed: 19306266]
7. Liu Z, Huang F, Du J, Shu W, Feng H, Xu X and Chen Y, Biomicrofluidics, 2013, 7, 11801. [PubMed: 24396522]
8. Augustsson P, Magnusson C, Nordin M, Lilja H and Laurell T, Anal. Chem, 2012, 84, 7954–7962. [PubMed: 22897670]
9. Phillips JA, Xu Y, Xia Z, Fan ZH and Tan W, Anal. Chem, 2009, 81, 1033–1039. [PubMed: 19115856]
10. Mittal S, Wong IY, Deen WM and Toner M, Biophys. J, 2012, 102, 721–730. [PubMed: 22385842]
11. Hyun KA, Lee TY and Jung H, Il, Anal. Chem, 2013, 85, 4439–4445. [PubMed: 23521012]
12. Han KN, Li CA and Seong GH, Annu. Rev. Anal. Chem, 2013, 6, 119–141.
13. Chen P, Huang Y, Hoshino K and Zhang X, Lab Chip, 2014, 14, 446–458. [PubMed: 24292816]
14. Zborowski M and Chamers JJ, Anal. Chem, 2011, 83, 8050–8056. [PubMed: 21812408]
15. Gratton SEA, Ropp PA, Pohlhaus PD, Luft JC, Madden VJ, Napier ME and DeSimone JM, Proc. Natl. Acad. Sci. U.S.A, 2008, 105, 11613–11618. [PubMed: 18697944]
16. Blanco E, Shen H and Ferrari M, Nat. Biotechnol, 2015, 33, 941–951. [PubMed: 26348965]
17. Nel AE, Mädler L, Velegol D, Xia T, V Hoek EM, Somasundaran P, Klaessig F, Castranova V and Thompson M, Nat. Mater, 2009, 8, 543–557. [PubMed: 19525947]
18. Petros RA and Desimone JM, Nat. Rev. Drug Discov, 2010, 9, 615–627. [PubMed: 20616808]
19. Hao NJ, Li LF and Tang FQ, Int. Mater. Rev, 2017, 62, 57–77.
20. Hao N, Li L and Tang F, Biomater. Sci, 2016, 4, 575–591. [PubMed: 26818852]
21. Geng Y, Dalhaimer P, Cai SS, Tsai R, Tewari M, Minko T and Discher DE, Nat. Nanotechnol, 2007, 2, 249–255. [PubMed: 18654271]
22. Yang K and Ma YQ, Nat. Nanotechnol, 2010, 5, 579–583. [PubMed: 20657599]
23. Elvira KS, Casadevall i Solvas X, Wootton RCR and de Mello AJ, Nat. Chem, 2013, 5, 905–915. [PubMed: 24153367]
24. Hao N, Nie Y, Shen T and Zhang XJ, Lab Chip, 2018, 18, 1997–2002. [PubMed: 29923569]

25. Valencia PM, Farokhzad OC, Karnik R and Langer R, Nat. Nanotechnol, 2012, 7, 623–629. [PubMed: 23042546]
26. Zhao C-X, He L, Qiao SZ and Middelberg APJ, Chem. Eng. Sci, 2011, 66, 1463–1479.
27. Park J, Il, Saffari A, Kumar S, Günther A and Kumacheva E, Annu. Rev. Mater. Res, 2010, 40, 415–443.
28. Knauer A and Koehler JM, Nanotechnol. Rev, 2014, 3, 5–26.
29. Nie Y, Hao N and Zhang XJ, Sci. Rep, 2017, 7, 12616. [PubMed: 28974729]
30. Hao N, Nie Y and Zhang XJ, ACS Sustain. Chem. Eng, 2018, 6, 1522–1526.
31. Hao N, Nie Y, Tadimety A, Closson AB and Zhang XJ, Mater. Res. Lett, 2017, 5, 584–590.
32. Shin SJ, Kim YH, Kim CW, Cha HG, Kim YJ and Kang YS, Curr. Appl. Phys, 2007, 7, 404–408.
33. Kim J, Kim J, Kim J and Hyeon Kim K, J. Appl. Phys, 2013, 113, 2011–2014.
34. Li L, Guan Y, Liu H, Hao N, Liu T, Meng X, Fu C, Li Y, Qu Q, Zhang Y, Ji S, Chen L, Chen D and Tang F, ACS Nano, 2011, 5, 7462–7470. [PubMed: 21854047]
35. Chang Z, Wang Z, Shao D, Yue J, Xing H, Li L, Ge M, Li M, Yan H, Hu H, Xu Q and Dong W, ACS Appl. Mater. Interfaces, 2018, 10, 10656–10663. [PubMed: 29468874]
36. Schneck H, Gierke B, Uppenkamp F, Behrens B, Niederacher D, Stoecklein NH, Templin MF, Pawlak M, Fehm T and Neubauer H, PLoS One, 2015, 10, e0144535. [PubMed: 26695635]
37. Chen P, Huang Y-Y, Hoshino K and Zhang XJ, Sci. Rep, 2015, 5, 8745. [PubMed: 25735563]
38. Hoshino K, Huang Y-Y, Lane N, Huebschman M, Uhr JW, Frenkel EP and Zhang X, Lab Chip, 2011, 11, 3449–3457. [PubMed: 21863182]
39. Hoshino K, Chen P, Huang YY and Zhang X, Anal. Chem, 2012, 84, 4292–4299. [PubMed: 22510236]
40. Huang Y, Chen P, Wu C, Hoshino K, Sokolov K, Lane N, Liu H, Huebschman M, Frenkel E and Zhang XJ, Sci. Rep, 2015, 5, 16047. [PubMed: 26538094]
41. Chen J, Li J and Sun Y, Lab Chip, 2012, 12, 1753–1767. [PubMed: 22437479]

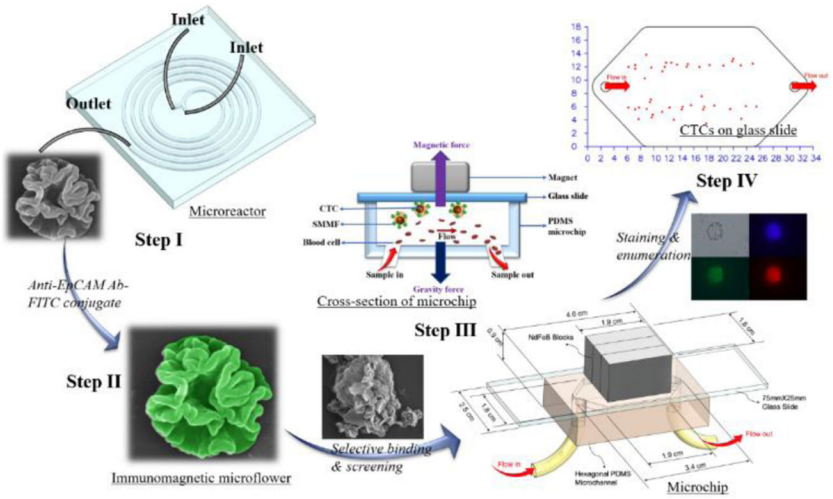

Figure 1.

Schematic workflow showing the step-by-step process of microfluidics-enabled synthesis of SMMF toward CTCs screening.

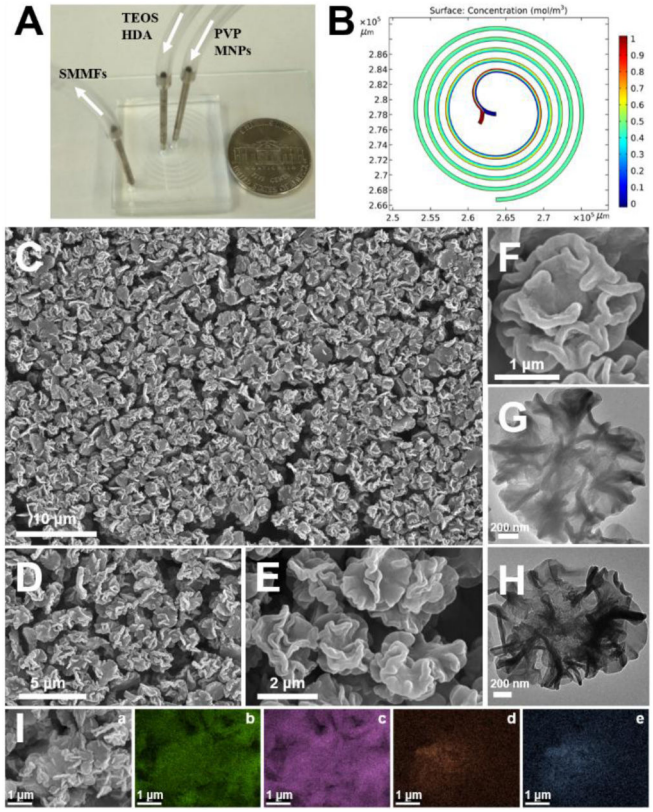

Figure 2.

Microfluidic synthesis and characterization of SMMF. (A) The photograph showing the microfluidic device used in this study, with a U.S. five cent coin for scale. (B) Simulation results demonstrating mixing at a flow rate of 4mL/min in microfluidic spiral channel, where two flows having different concentrations achieve complete mixing within about one run (see details in SI). (C-F) SEM image of hierarchical silica microflower at different magnifications. (G) and (H) showing TEM images of the as-synthesized silica microflower and FeCo-doped silica-magnetic microflower, respectively. (I) SEM image of SMMF (a) and the corresponding EDS elemental mapping analysis showing the presence of O (b), Si (c), Fe (d), and Co (e).

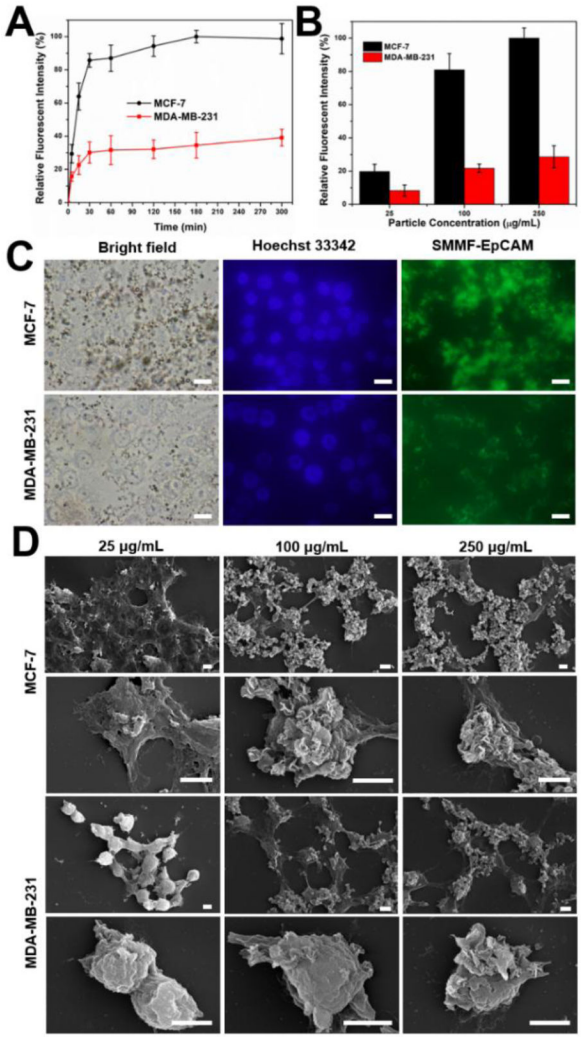

Figure 3.

Interactions of SMMF-EpCAM with MCF-7 and MDA-MB-231 cells. (A) Cellular binding kinetics of SMMF-EpCAM at a particle concentration of 100 μg/mL with MCF-7 and MDA-MB-231 cells over 300 min. (B) Cellular binding efficiency of SMMF-EpCAM at different particle concentrations for 30 min. (C) Bright-field and fluorescent microscopic images of cells exposed to SMMF-EpCAM (100 μg/mL) for 30 min. Scale bar = 20 μm. (D) SEM images of cells after treated with SMMF-EpCAM for 30 min. Scale bar = 5 μm.

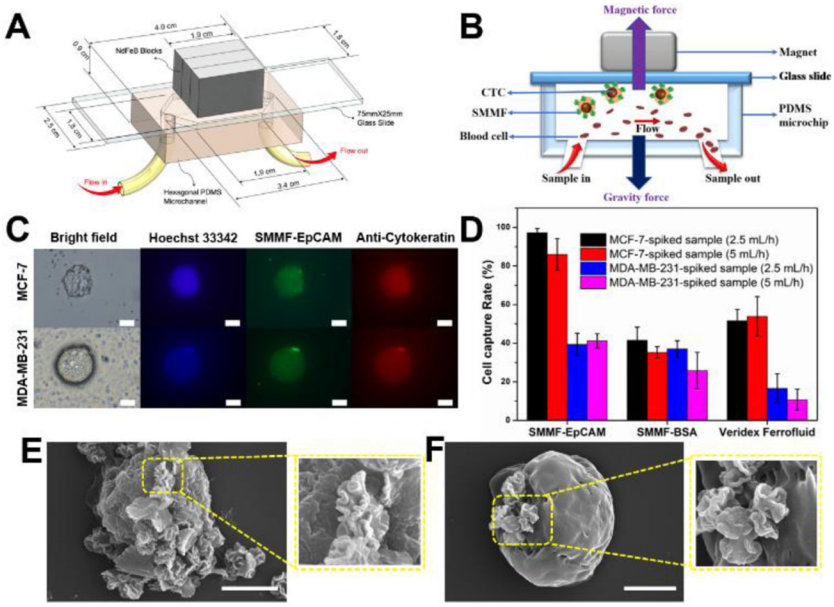

Figure 4.

Microfluidic screening of tumor cells with hierarchical microflower material. (A) Schematic image of our developed microchip for CTCs screening. (B) The cross-section of microchip for showing the working principle in this study. (C) Representative images of captured MCF-7 cell and MDA-MB-231 cell using SMMF-EpCAM. Scale bar = 20 μm. (D) Screening efficiency comparison of SMMF-EpCAM, SMMF-BSA, and Veridex Ferrofluid (from CellSearch™, see details in SI) at different screening flow rates for the tumor cells spiked in whole blood samples. (E) and (F) are the representative SEM images of SMMF-EpCAM-captured MCF-7 cell and MDA-MB-231 cell, respectively. Scale bar = 5 μm.